

# Electron spin precession in semiconductor quantum wires with Rashba spin-orbit coupling

Manuel Valín-Rodríguez, Antonio Puente and Llorenç Serra <sup>a</sup>

Departament de Física, Universitat de les Illes Balears, E-07122 Palma de Mallorca, Spain

April 16, 2003

**Abstract.** The influence of the Rashba spin-orbit coupling on the electron spin dynamics is investigated for a ballistic semiconductor quantum wire with a finite width. We monitor the spin evolution using the time-dependent Schrödinger equation. The pure spin precession characteristic of the 1D limit is lost in a 2D wire with a finite lateral width. In general, the time evolution in the latter case is characterized by several frequencies and a nonrigid spin motion.

**PACS.** 73.21.Hb Quantum wires – 73.22.Dj Single particle states

## 1 Introduction

The control of the Rashba spin-orbit coupling is one of the most promising tools for the manipulation of the spin of the carriers within semiconductor heterostructures. In the last years, there have appeared several proposals of spin-based devices relying on this mechanism [1,2]. Among them we cite the spin-FET, first proposed by Datta and Das [3], the spin filters [4] and the spin guides [5].

The origin of the Rashba spin-orbit coupling in III-V semiconductor heterostructures lies in their asymmetry. The lack of space symmetry causes a local electric field perpendicular to the plane of the heterostructure. The associated relativistic correction makes the electrons feel an effective magnetic field which separates in energy the different spin states [6]. This dependence of the Rashba spin-orbit coupling on the interface electric field remains as a great advantage for spin control in semiconductors. Indeed, the intensity of the coupling can be controlled by applying a vertical electric field to the heterostructure, as proved experimentally by Nitta *et al.* [7].

In this work, we shall focus on the spin precessional properties of conduction electrons in a quantum wire having a finite width. The problem of the quantum wire with Rashba coupling has already been studied by Moroz and Barnes [8], who addressed the ballistic conductance and the subband structure of the wire; and by Mireles and Kirichenow [9], who analyzed the spin-dependent transport within a tight binding model. Following a different approach, Governale and Zülicke [10] have also treated the problem, and, more recently, Egues *et al.* [11] have proposed to take advantage of the coupling of the first two transverse subbands to create a spin-FET with enhanced spin control. In this work, we shall concentrate on how the

coupling of the different transverse subbands, due to the Rashba term, affects the electron spin precession.

The Hamiltonian representing the Rashba spin-orbit coupling in terms of the electron momentum ( $\mathbf{p}$ ) and the Pauli matrices ( $\sigma$ 's) reads

$$\mathcal{H}_{SO} = \frac{\lambda_R}{\hbar} (p_y \sigma_x - p_x \sigma_y), \quad (1)$$

where  $\lambda_R$  represents the intensity of the spin-orbit coupling, depending on the heterostructure's vertical electric field. To stress the experimental feasibility we have assumed a value  $\lambda_R = 1.03 \times 10^{-9}$  eV cm, as reported in Ref. [7] for an  $\text{In}_{0.53}\text{Ga}_{0.47}\text{As}/\text{In}_{0.52}\text{Al}_{0.48}\text{As}$  quantum well. Other experimental parameters corresponding to this sample are:  $m^* = 0.05 m_e$ ,  $\epsilon = 13.9$  for InGaAs, and the Fermi wavevector  $k_F = 3.5 \times 10^6$  cm<sup>-1</sup>, corresponding to a 2DEG density  $n_s \simeq 2 \times 10^{12}$  cm<sup>-2</sup>. All calculations discussed below have been obtained using this parameter set.

We assume a wire oriented along the  $y$  axis with confinement achieved in the  $x$  direction. In the simplified model of a one-dimensional wire the terms containing  $x$  or  $p_x$  are dropped and the remaining Hamiltonian

$$\mathcal{H}_{1D} = \frac{p_y^2}{2m^*} + \frac{\lambda_R}{\hbar} p_y \sigma_x \quad (2)$$

is compatible with the observables  $\{p_y, \sigma_x\}$ . That is, the energy eigenstates are characterized by their  $x$  spin component and  $y$  momentum ( $\hbar k_y$ ). In this system, the state of an electron having well-defined momentum and with arbitrary spin orientation decomposes into a combination of the spin eigenstates  $|s_x+\rangle$  and  $|s_x-\rangle$ , leading to a spin *precessional* motion about the  $x$  axis, i.e., in the  $S_y$ - $S_z$  plane. The spin evolution is characterized by an angular frequency  $\omega_P$ , corresponding to the energy difference

<sup>a</sup> E-mail: e-mail: DFSLSC4@clust.uib.es

between the two spin eigenstates,  $\hbar\omega_P = 2\lambda_R k_y$ . This precession frequency leads to the well-known formula for the angular modulation of spin orientation  $\theta_R = 2m^* \lambda_R L / \hbar^2$ , for a channel length  $L$ .

When a two-dimensional free motion of the electrons is considered, the eigenstates of the Hamiltonian

$$\mathcal{H}_{2D} = \frac{(p_x^2 + p_y^2)}{2m^*} + \frac{\lambda_R}{\hbar} (p_y \sigma_x - p_x \sigma_y) \quad (3)$$

have again well-defined momentum  $\hbar\mathbf{k}$  and spin orientation, but the latter depends now on the wavevector  $\mathbf{k}$ . Using spinorial notation in the usual basis of  $|+\rangle$  and  $|-\rangle$  states for the  $S_z$  spin component, the wave functions and energies for a given  $\mathbf{k}$  read

$$\chi_{\mathbf{k}\pm} = e^{i\mathbf{k}\cdot\mathbf{r}} \begin{pmatrix} 1 \\ \mp i e^{i\phi} \end{pmatrix}, \quad (4)$$

$$\varepsilon_{\mathbf{k}\pm} = \frac{\hbar^2}{2m^*} (k_x^2 + k_y^2) \pm \lambda_R |\mathbf{k}|, \quad (5)$$

where  $\phi = \text{atan}(k_y/k_x)$  is the polar angle for  $\mathbf{k}$ . Note that the spinors (4) are eigenstates of a spin component orthogonal to  $\mathbf{k}$ , i.e., the spin orientation depends on the spatial wavevector, always pointing in perpendicular direction to  $\mathbf{k}$ . As in the 1D case, a state having well-defined momentum  $\hbar\mathbf{k}$  and arbitrary spin orientation decomposes into a linear combination of the above 2D eigenspinors  $\chi_{\mathbf{k}\pm}$ . Therefore, the evolution under  $\mathcal{H}_{2D}$  leads again to a spin precession of frequency  $\omega_P$  given by the energy difference between the corresponding 'up' and 'down' eigenstates. Namely,  $\hbar\omega_P = 2\lambda_R |\mathbf{k}|$ ; the same result of the 1D case. An important difference is, however, that the plane of spin precession depends in 2D on the spatial orientation of  $\mathbf{k}$ . Having analyzed the bulk limits, the question that arises is how the above *pure* spin precession is modified when the complete translational invariance of the homogeneous 1D and 2D systems is lost in a wire with a finite width.

## 2 The Model

In order to model the quantum wire we maintain the translational invariance in the longitudinal coordinate ( $y$ ) while, in the transversal direction ( $x$ ) this symmetry is broken by a parabolic confinement

$$V(x) = \frac{1}{2} m^* \omega_0^2 x^2, \quad (6)$$

where  $\omega_0$  determines the *width* of the wire. The Hamiltonian representing the quantum wire reads

$$\mathcal{H} = \frac{\mathbf{p}^2}{2m^*} + \frac{1}{2} m^* \omega_0^2 x^2 + \frac{\lambda_R}{\hbar} (p_y \sigma_x - p_x \sigma_y). \quad (7)$$

As our system still retains one spatial symmetry we can reduce the spinorial 2D problem to a 1D one by factorizing out the  $y$  dependence,

$$\begin{pmatrix} \psi_{nk_y\uparrow}(\mathbf{r}) \\ \psi_{nk_y\downarrow}(\mathbf{r}) \end{pmatrix} = e^{ik_y y} \begin{pmatrix} \phi_{nk_y\uparrow}(x) \\ \phi_{nk_y\downarrow}(x) \end{pmatrix}. \quad (8)$$

The continuum index  $k_y$  in Eq. (8) labels the state of free motion in longitudinal direction while the discrete index  $n$  accounts for the different transversal subbands of the confining dimension. Introducing this general form of energy eigenspinor we obtain the reduced Hamiltonian for the spinorial transverse dependence.

$$\mathcal{H}_{tr} = \frac{\hbar^2 k_y^2}{2m^*} + \frac{p_x^2}{2m^*} + \frac{m^* \omega_0^2}{2} x^2 + \frac{\lambda_R}{\hbar} (\hbar k_y \sigma_x - p_x \sigma_y) \quad (9)$$

The transverse Hamiltonian, Eq. (9), can be analyzed by seeking direct solutions to the stationary Schrödinger equation or, equivalently, solving the time-dependent Schrödinger equation for given initial conditions. We shall use the latter approach since it yields a suitable scenario to address the dynamical spin evolution. For a given wavevector  $k_y$  the coupled time-dependent equations for the two spin components of any spinorial wavepacket:  $f_{k_y\uparrow}(x)$  and  $f_{k_y\downarrow}(x)$  read

$$i\hbar\partial_t \begin{pmatrix} f_{k_y\uparrow}(x, t) \\ f_{k_y\downarrow}(x, t) \end{pmatrix} = \begin{pmatrix} \mathcal{H}_0^{(x)} & \lambda_R (k_y + \partial_x) \\ \lambda_R (k_y - \partial_x) & \mathcal{H}_0^{(x)} \end{pmatrix} \begin{pmatrix} f_{k_y\uparrow}(x, t) \\ f_{k_y\downarrow}(x, t) \end{pmatrix}, \quad (10)$$

where

$$\mathcal{H}_0^{(x)} = -\frac{\hbar^2}{2m^*} \partial_x^2 + \frac{m^* \omega_0^2}{2} x^2. \quad (11)$$

Note that in  $\mathcal{H}_0^{(x)}$  we have dropped the longitudinal kinetic contribution, not important for time evolution.

It is well known that in quantum mechanics time evolution can provide complete information about the stationary states of a Hamiltonian through spectral analysis. Indeed, for a time-independent Hamiltonian an arbitrary wavepacket can be expanded as a series in the stationary energy eigenstates

$$\begin{pmatrix} f_{k_y\uparrow}(x, t) \\ f_{k_y\downarrow}(x, t) \end{pmatrix} = \sum_n A_{nk_y} e^{-\frac{i}{\hbar} \varepsilon_{nk_y} t} \begin{pmatrix} \phi_{nk_y\uparrow}(x) \\ \phi_{nk_y\downarrow}(x) \end{pmatrix}. \quad (12)$$

Using the fast Fourier transform (FFT) we can extract the harmonic frequencies ( $\varepsilon_{nk_y}$  energies) from the evolution of an arbitrary wavepacket. Furthermore, if this analysis is repeated at different spatial points the space components of the energy eigenspinor  $\phi_{nk_y\uparrow}(x)$  and  $\phi_{nk_y\downarrow}(x)$ , can also be obtained.

## 3 Results

The Hamiltonian of Eq. (7), apart from kinetic and potential terms, contains the longitudinal and transversal spin-orbit contributions coupling  $x$  and  $y$  spatial motions with the electron spin. It is worth noticing that there is an analytical limit to the solution of Eq. (10) when  $p_x f_{k_y} \ll \hbar k_y f_{k_y}$ . In this case the solutions are similar to

those discussed above for  $\mathcal{H}_{1D}$ , i.e., the eigenstates are still plane waves in  $y$  direction with spin oriented along  $x$  but now with an harmonic oscillator transverse profile. The corresponding energy spectrum is also analytically known

$$\varepsilon_{nk_y s}^{(0)} = \frac{\hbar^2 k_y^2}{2m^*} + \left(n + \frac{1}{2}\right) \hbar\omega_0 + \lambda_R k_y s, \quad (13)$$

where  $s = +1$  for  $+x$  spin orientation (up) and  $s = -1$  for  $-x$  (down). If we subtract the longitudinal kinetic term  $\hbar^2 k_y^2 / 2m^*$ , common to both spin orientations, the remaining band structure consists of doubly split transverse subbands, linear in  $k_y$  and having a common origin at  $(n + 1/2)\hbar\omega_0$ . Another analytical limit can be obtained neglecting  $\lambda_R p_y \sigma_x$  in (7); in this case, spin-orbit interaction only produces a little constant shift in the energy levels that does not depend on spin orientation.

As a check of our numerical procedure, Fig. 1 shows the results for a simulation using the above simplified Hamiltonian (neglecting  $\lambda_R p_x \sigma_y$  in Eq. (7)). The parameters used are:  $\hbar\omega_0 = 3.5$  meV,  $k_y = 1.0 \times 10^6$  cm $^{-1}$  and the above mentioned spin-orbit intensity. The initial input for the time-evolution is a Gaussian-shaped wavepacket having spin oriented in  $+z$ ,

$$\begin{pmatrix} f_{k_y \uparrow}(x, 0) \\ f_{k_y \downarrow}(x, 0) \end{pmatrix} \equiv \frac{1}{2\sigma\sqrt{\pi}} e^{-\frac{(x-x_0)^2}{2\sigma^2}} \begin{pmatrix} 1 \\ 0 \end{pmatrix}. \quad (14)$$

Using a finite  $x_0$  and  $\sigma \simeq \sqrt{\frac{\hbar}{m^* \omega_0}}$  we ensure that the initial wavepacket is composed of several transversal eigenstates in the low energy region. Figure 1 shows the spectrum corresponding to the wavepacket's oscillations at an arbitrary  $x$  point, as well as the transversal densities extracted for the two lowest peaks. An excellent agreement between numerical and analytical energies and eigen-spinors is found. Figure 2 represents the dynamical spin evolution for the above initial spinor, corresponding to a pure precession in excellent agreement with the analytical frequency  $\hbar\omega_P = 2\lambda_R k_y$ .

Note that, in this analytical regime, spin precession is independent of the transversal state, as the energy gaps are common to the different subbands. This statement implies that spin evolution is independent of the transversal profile of the injected particles. Numerically, we have checked that arbitrary initial profiles for the  $x$  dependence lead to the same spin dynamics.

The above analytical regime no longer holds when the transverse motion couples with the spin through the term  $\lambda_R p_x \sigma_y$  in Eq. (7). Complete analytical solutions for the Hamiltonian including the full spin-orbit interaction are not available and numerical calculations are needed to solve the problem. The first question arising is how the band structure of the simplified Hamiltonian is modified when transversal spin-orbit coupling is included. Figure 3 shows the corresponding band structure for the same wire parameters considered above. In order to clarify the effect of the transversal coupling the longitudinal kinetic term  $\hbar^2 k_y^2 / 2m^*$  has been subtracted and the analytical energies are shown with dotted lines. It can be seen that for low

values of  $k_y$  there is good agreement between the simplified and full Hamiltonians; but this is not true when we approach a region of band crossings. When the  $(n + 1)$ -th down subband reaches the up branch of the  $n$ -th subband, the transversal coupling produces a large effect, removing the band degeneracy and opening a gap between these two branches,  $(n + 1, \downarrow)$  and  $(n, \uparrow)$  [8]. The gap opened clearly depends on the transversal subbands involved; the higher transversal state the larger the gap, as easily noticed from Fig. 3. It can also be observed that the range of  $k_y$ 's where there is a good agreement between full calculations and analytical model diminishes as the subband index increases. These changes on the level structure suggest significant modifications of the spin precession due to the coupling with transversal motion.

As shown by Fig. 3, transversal coupling effects maximize at the analytical model crossings, occurring approximately when  $2\lambda_R k_y = \hbar\omega_0$ . The fulfillment of this condition establishes a rough criterion to quantify the relevance of the transversal spin-orbit coupling. Nevertheless, it must be also stressed that the coupling depends sensitively on the subband index  $n$ .

The influence of the transversal coupling can also be observed in the structure of the eigen-spinors. In the analytical model the eigenfunctions are states having well-defined spin orientation. The transversal spin-orbit coupling mixes the different subbands leading to a more complex structure of the eigenstates. Figure 4 represents the densities corresponding to three lowest eigenstates in the region of maximum band anticrossing, i.e.,  $k_y = 1.70 \times 10^6$  cm $^{-1}$ . The lowest energy state corresponds to a branch without crossings and, therefore, its eigenvalue and eigen-spinor are very similar to those of the analytical model; spin density mainly oriented in  $-x$  direction with a residual structure in  $z$  orientation. The other two eigen-spinors differ substantially from those of the analytical model; spin has no predominant orientation and displays a complex texture very similar to those found in Ref. [10]. Charge and spin densities are related to the eigen-spinor components through the usual expressions

$$\begin{aligned} \rho(x) &= |\phi_{nk_y \uparrow}(x)|^2 + |\phi_{nk_y \downarrow}(x)|^2 \\ m_z(x) &= |\phi_{nk_y \uparrow}(x)|^2 - |\phi_{nk_y \downarrow}(x)|^2 \\ m_x(x) &= 2\text{Re} \left\{ \phi_{nk_y \uparrow}(x) \phi_{nk_y \downarrow}^*(x) \right\}. \end{aligned} \quad (15)$$

Until now we have presented the effects produced by the full spin-orbit coupling on the level scheme with respect to the analytical model, having results in good agreement with those of Ref. [8]. The question that we address next is how this modified band structure reflects on the spin dynamics. We consider first the case of a particle having well-defined spin orientation at initial time and  $y$ -momentum in the range of band anticrossings, i.e., an spinor as in (12) evolving with  $k_y = 1.70 \times 10^6$  cm $^{-1}$  in Eq. (10). The initial condition thus reads

$$f_{k_y}(x, 0) \equiv \frac{1}{\pi^{1/4}} \left[ \frac{m^* \omega_0}{\hbar} \right]^{1/4} e^{-\frac{m^* \omega_0}{2\hbar} x^2} \begin{pmatrix} 1 \\ 0 \end{pmatrix}. \quad (16)$$

The spatial part of this injected spinor is equal to that of the lowest analytic subband. In this way, we ensure that it is in the low energy range, very close to the first transversal subband.

The dynamical evolution of this injected particle is shown in Fig. 5. The spin trajectory on the  $S_y$ - $S_z$  plane is quite involved, manifesting a multifrequential evolution. Indeed, the Fourier transform of the series shows that spin evolves in time as a superposition of several frequencies corresponding to the energy transitions between the different anticrossed branches. Since the gap opened by the transversal spin-orbit coupling varies from one subband to another, several precession frequencies are found in the anticrossing region. On the contrary, the analytical model predicts a common transition energy for all the transversal subbands (see Fig. 3), leading to a unique precession frequency. This feature proves that spin evolution in 2D wires noticeably depends on the transversal state of the particle. In the particular case of Fig. 5 the precession is characterized by two dominant frequencies, corresponding to the transitions between the lowest branch and the next two higher branches, represented by dark-gray arrows in Fig. 3. This two-frequency evolution yields a variable spin amplitude, in agreement with the displayed trajectory. The spin-orbit coupling makes the precessional frequencies depend on  $k_y$  in a non-trivial way. At the same time, it gives rise to a  $k_y$ -dependent spin modulation angle that would lead to a certain degree of decoherence in the spin transport through the wire.

Figure 6 shows the precessional spectra corresponding to an initial spinor having well-defined spin (in  $+z$  direction) and different transversal states. The precessional spectrum corresponding to the first transversal subband ( $n = 0$ ) is that represented in Fig. 5. The precessional spectra for the higher transversal states,  $n = 1$  and  $n = 2$ , exhibit an enhanced multi-frequential character, since more transitions significantly contribute to the spin evolution. It can also be seen that the strength spreads over a higher frequency interval as the subband index  $n$  is increased. For low  $k_y$ 's, out of the anticrossing region, the spin evolution recovers a single-frequency behaviour, with slight deviations from the analytical results (cf. Fig. 2). Note that, in general, a pure up ( $+z$ ) spin injected into the wire will couple with the different spinor eigenstates and, therefore, the multifrequential evolution can not be avoided.

Another question of relevance is how the transversal size influences the precession. From Fig. 4 we can estimate the width of the wire in 90 – 120 nm for  $\hbar\omega_0 = 3.5$  meV. If we reduce the value of  $\omega_0$  and maintain the intensity of spin-orbit coupling the crossings of transversal bands become more frequent as subbands are less spaced. Figure 7 shows the corresponding band structure in the case  $\hbar\omega_0 = 0.70$  meV; from the densities of the eigenspinors an estimated width of 200 – 250 nm can be obtained for this wire. Deviations from the analytical band structure are clearly visible in spite of the reduced  $k_y$  range displayed. This feature is reflected in the precessional spectra which are fragmented even for relatively low  $k_y$ 's. By contrast,

a wire of  $\hbar\omega_0 = 14$  meV, having an estimated width of 40 – 60 nm, shows a band structure very close to that of the analytical decoupled Hamiltonian, as displayed in Fig. 8. This also reflects on the precessional spectra, which are single-moded and match the value given by the analytical formula  $\hbar\omega_P = 2\lambda_R k_y$ .

In practical implementations of the Datta and Das spin transistor [3] the above discussed spin decoherence at subband crossings would strongly affect the device operation and, therefore, it should be carefully considered in the design of appropriate working parameters. We can quantify the decoherence by representing the spin amplitude after the first spin flip, i.e., after the first  $\pi$  rotation. Figure 9 represents this quantity as a function of wire width ( $\omega_0$ ) for a  $k_y$  value in the anticrossing region,  $\approx \hbar\omega_0/2\lambda_R$ . It can be seen that as the wire becomes wider (lower  $\omega_0$ ), the multi-frequential precession leads to an important reduction of the  $z$  spin after the first inversion.

## 4 Summary

In summary, we have studied the electronic spin precession in quantum wires with Rashba spin-orbit coupling by means of real time simulations. A detailed study of the band structure for this system has been presented and compared with a decoupled analytical model. It has been shown that deviations from the simple spin precession regime are determined by the relative importance of the longitudinal spin-orbit energy ( $\lambda_R k_y$ ) and the transversal confining energy ( $\hbar\omega_0$ ) and that the spin precession fragments into several frequencies whose weights depend on the transversal state of the particle. The dependence of the spin precession on the wire width has also been studied and illustrated through the band structure.

This work was supported by Grant No. BFM2002-03241 from DGI (Spain).

## References

1. X. F. Wang, P. Vasilopoulos, F. M. Peeters, Appl. Phys. Lett. **80** 1400 (2002).
2. J. C. Egues, G. Burkard and D. Loss, Phys. Rev. Lett. **89**, 176401 (2002).
3. S. Datta and B. Das, Appl. Phys. Lett. **56**, 665 (1990).
4. T. Koga, J. Nitta, H. Takayanagi, S. Datta, Phys. Rev. Lett. **88**, 126601 (2002).
5. M. Valín-Rodríguez, A. Puente and Ll. Serra, cond-mat/0211694.
6. E. I. Rashba, Fiz. tverd. Tela (Leningrad) **2**, 1224 (1960) [Sov. Phys. Solid State **2**, 1109 (1960)].
7. J. Nitta, T. Akazaki, H. Takayanagi and T. Enoki, Phys. Rev. Lett. **78** 1335 (1997).
8. A. V. Moroz and C. H. W. Barnes, Phys. Rev. B **60** 14272 (1999).
9. F. Mireles and G. Kirczenow, Phys. Rev. B **64** 024426 (2001).
10. M. Governale and U. Zülicke, Phys. Rev. B **66**, 073311 (2002).
11. J. C. Egues, G. Burkard and D. Loss, Appl. Phys. Lett. **82**, 2658 (2003).

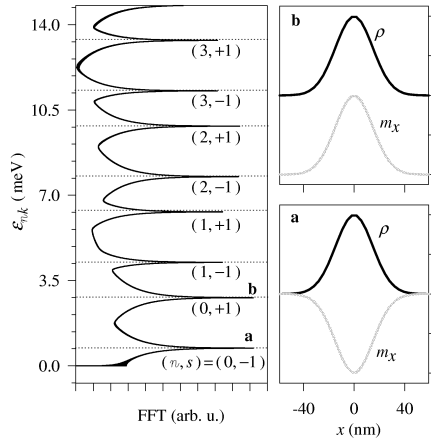


**Fig. 1.** Fast Fourier transform (FFT) in logarithmic scale corresponding to the oscillations of a *injected* wavepacket evolving with the simplified Hamiltonian (without transversal spin-orbit coupling). Dotted lines indicate the analytical eigenvalues labeled by the transversal subband index  $n$  and spin orientation  $s$ . Right panels show the non-zero densities corresponding to the two lowest eigenstates; charge and spin densities have been shifted in panel **b** to better distinguish them.

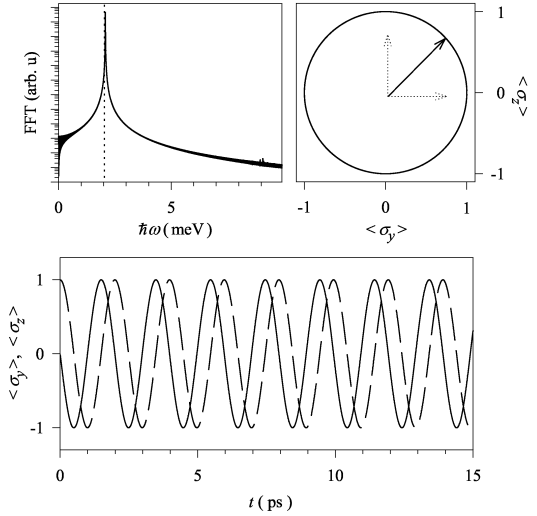


**Fig. 2.** Lower panel: time-evolution of the spin expectation values in the  $S_y - S_z$  plane. Upper-left panel: Fourier spectrum (logarithmic scale) corresponding to the  $\langle \sigma_z \rangle(t)$  time series. The dotted line gives the analytical energy. Upper-right panel: trajectory in the  $S_y - S_z$  plane of the  $\langle \sigma \rangle$  vector.

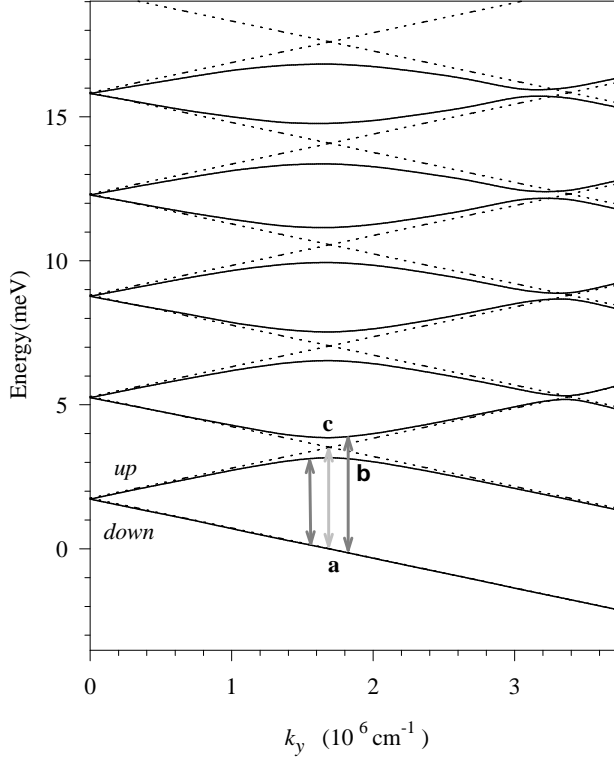


**Fig. 3.** Band structure, excluding the constant kinetic term  $\hbar^2 k_y^2 / 2m^*$ , corresponding to the first five transversal subbands of a wire with  $\hbar\omega_0 = 3.5$  meV. Results for the full Hamiltonian (solid lines) and for the decoupled one (dotted lines) are shown. Transitions from the lowest down branch in the decoupled (light grey) and full (dark grey) models are indicated by arrows.

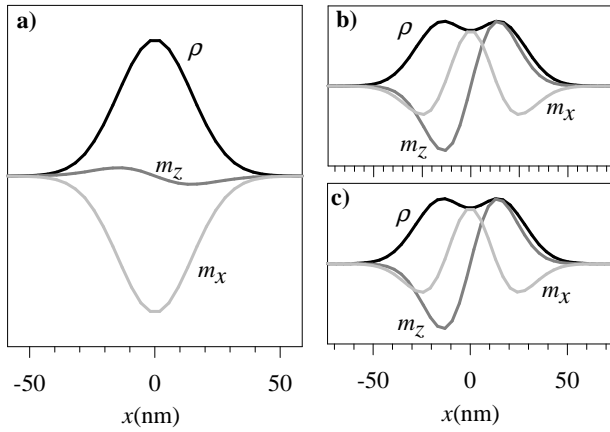


**Fig. 4.** Charge and spin transversal profiles for the three lowest eigenstates of the full Hamiltonian in the anticrossing region. The panel labels correspond to the **a**, **b** and **c** branches indicated in Fig. 3.

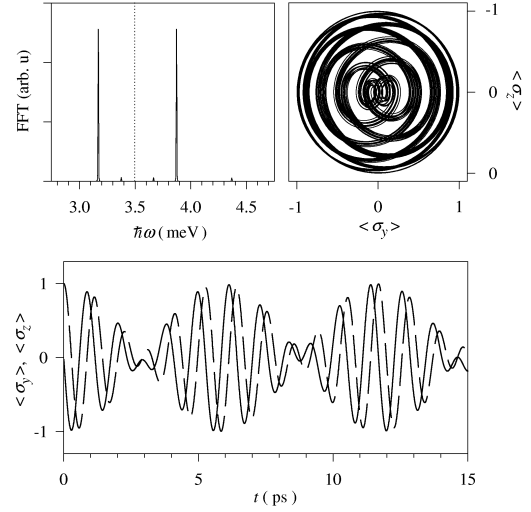


**Fig. 5.** Lower panel: time-evolution of the  $\langle\sigma_y\rangle$  and  $\langle\sigma_z\rangle$  expectation values for an injected wave-packet with well-defined initial  $z$  spin orientation using the full Hamiltonian. Upper-left panel: Fast Fourier transform (linear scale) of the  $\langle\sigma_z\rangle(t)$  series; the dotted line indicates the precession frequency given by  $\hbar\omega_P = 2\lambda_R k_y$ . Upper-right panel: trajectory in the  $S_y$ - $S_z$  plane of the  $\langle\sigma\rangle$  vector.

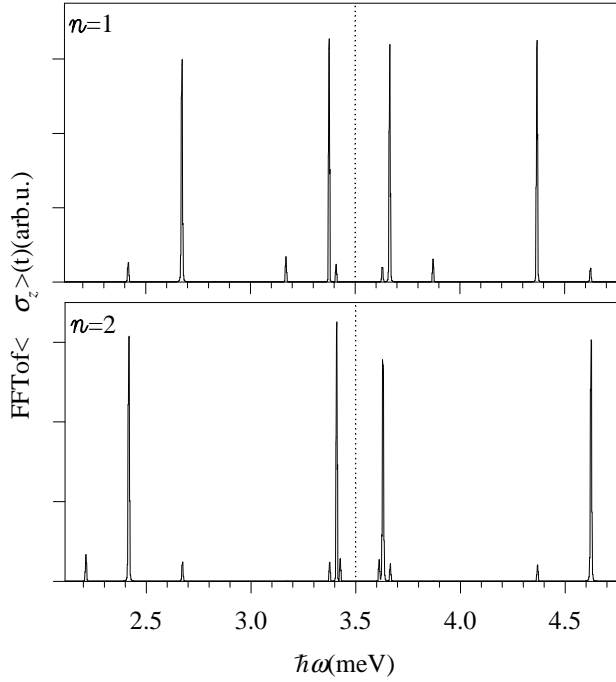


**Fig. 6.** Precessional spectra obtained from the time-evolution of harmonic spinors with well-defined  $z$  spin corresponding to the  $n = 1$  and 2 transversal subbands in the anticrossing region. Dotted lines indicate the energy  $\hbar\omega_P$ .

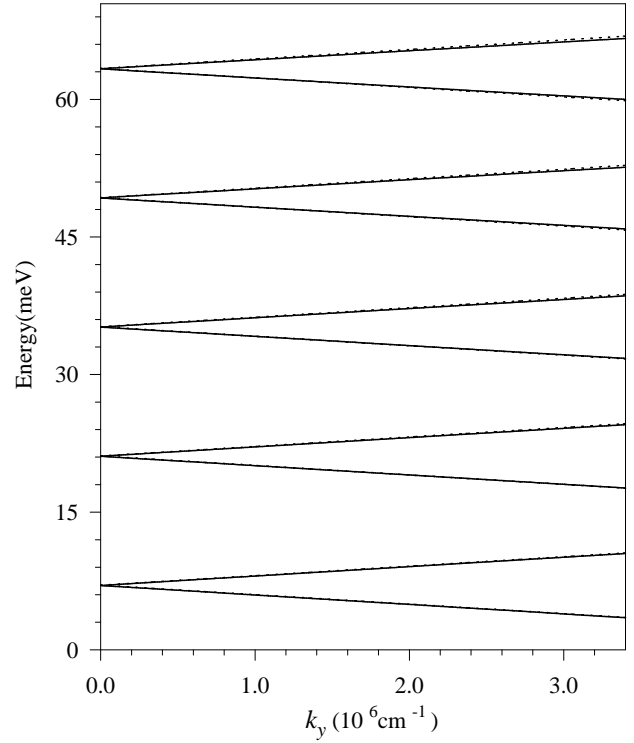


**Fig. 8.** Same as Fig. 7 but for  $\hbar\omega_0 = 14$  meV (Note the enlarged  $k_y$ -scale with respect to Fig. 7).

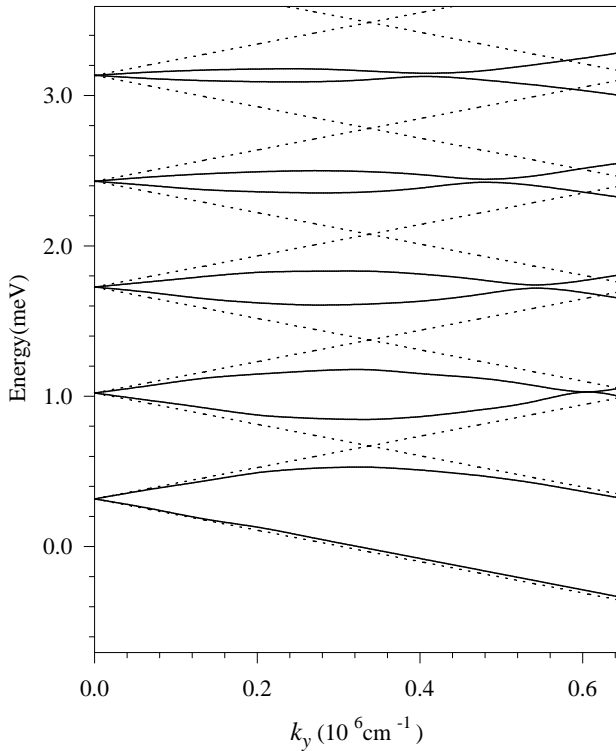


**Fig. 7.** Band structure without the longitudinal kinetic term  $\hbar^2 k_y^2 / 2m^*$  corresponding to the first five transversal subbands of a wire with  $\hbar\omega_0 = 0.7$  meV for the full Hamiltonian (solid lines) and for the decoupled one (dotted lines).

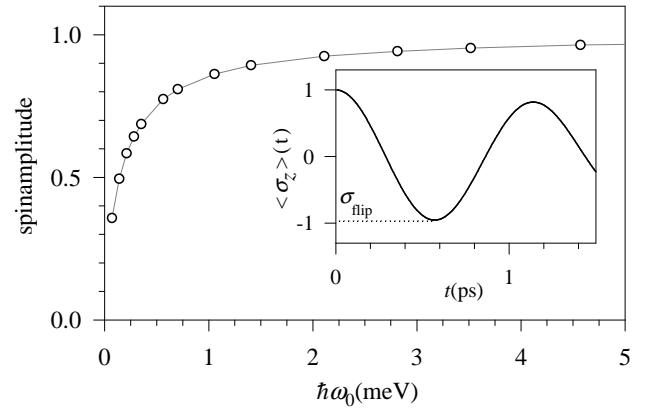


**Fig. 9.** Amplitude of the  $\langle \sigma_z \rangle(t)$  signal after the first spin flip as a function of the transversal confinement strength  $\hbar\omega_0$ . The inset illustrates the displayed quantity for the case  $\hbar\omega_0 = 3.5$  meV.